Low-breakdown-voltage solar cells for shading-tolerant photovoltaic modules

Calcabrini, Andres; Procel Moya, Paul ; Kambhampati, Viswambhe; Manganiello, Patrizio; Muttillo, Mirco; Zeman, Miro; Isabella, Olindo

DOI
10.1016/j.xcrp.2022.101155

Publication date
2022

Document Version
Final published version

Published in
Cell Reports Physical Science

Cell Reports
Physical Science

CellPress
OPEN ACCESS

Article

Low-breakdown-voltage solar cells for shading-tolerant photovoltaic modules

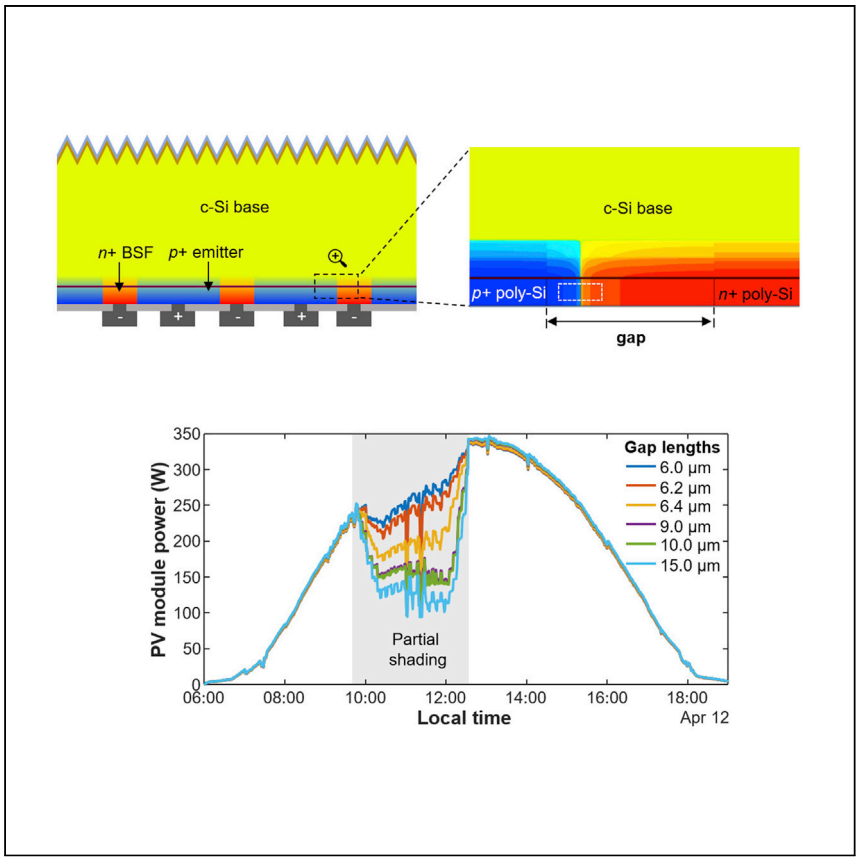

Calcabrini et al. explore the potential of low breakdown voltage solar cells to improve the shading tolerance of photovoltaic modules. They show that low breakdown voltage solar cells can significantly improve the electrical performance of partially shaded photovoltaic modules and can limit the temperature increase in reverse-biased solar cells.

Andres Calcabrini, Paul Procel Moya, Ben Huang, ..., Mirco Muttillo, Miro Zeman, Olindo Isabella

p.manganiello@tudelft.nl

Highlights

The p+/n+ regions in back-contacted cells enable tunneling under reverse bias

The energy yield of shaded photovoltaic modules could be increased up to 20%

Experiments with commercial low-breakdown-voltage cells show 4% yield improvement

Calcabrini et al., Cell Reports Physical Science 3, 101155
December 21, 2022
https://doi.org/10.1016/j.xcrp.2022.101155

Cell Reports
Physical Science

CellPress
OPEN ACCESS

Article

Low-breakdown-voltage solar cells for shading-tolerant photovoltaic modules

Andres Calcabrini,[1] Paul Procel Moya,[1] Ben Huang,[1] Viswambher Kambhampati,[1] Patrizio Manganiello,[1,2,*] Mirco Muttillo,[1] Miro Zeman,[1] and Olindo Isabella[1]

SUMMARY

The integration of photovoltaic (PV) technology in urban environments poses new challenges for the design of PV modules. In particular, the poor shading tolerance of conventional PV modules strongly limits the energy performance of urban PV systems. In this work, we analyze how interdigitated back-contact solar cells with low-breakdown voltages can help improve the shading tolerance of PV modules. Through detailed simulations, we show that the breakdown voltage can be tuned without significantly degrading the efficiency of the solar cell. Simulation results indicate that, under partial shading conditions, cells with a 0.3-V breakdown voltage could boost by 20% the annual yield of conventional crystalline silicon PV modules with three bypass diodes. These findings are supported by a four-month-long monitoring campaign of PV modules with different breakdown characteristics, which shows a specific yield gain of about 4% in PV modules with six bypass diodes.

INTRODUCTION

Over the last two decades, photovoltaic (PV) modules have been massively deployed all over the world. Although most PV modules have been installed in utility- and commercial-scale power plants, a significant number of PV generators has been installed in urban environments. Urban PV systems are traditionally installed on rooftops but more recently also on façades and building infrastructure.[1,2]

Urban PV systems frequently face east or west and are exposed to uneven illumination conditions because of bird droppings, leaves, and shading caused by trees and building structures in the vicinity of the PV modules. These suboptimal conditions significantly limit the system's electrical performance.[3] In view of an increasing integration of PV technology in urban environments, not only in building structures but also in vehicles,[4] development of shading-tolerant PV modules is becoming a pressing issue to maximize the yield of urban PV systems.[5]

Typically, all solar cells in wafer-based PV modules are connected in series, forming strings to limit the module's output current and minimize joule losses in cables and power converters. However, strings of solar cells perform poorly under non-uniform illumination. One of the main factors that affects the shading tolerance of a PV module is the reverse current-voltage (I-V) characteristics of its solar cells. Most crystalline Si solar cells have a breakdown voltage (BDV) between −10 and −30 V.[6–8]

Because of the large (absolute) BDV, shaded solar cells restrict the current flow and power output of the entire string of cells. When a shaded cell is driven into

[1]Photovoltaic Materials and Devices Group, Department of Electrical Sustainable Energy, Delft University of Technology, Postbus 5031, Delft, 2600 GA Zuid-Holland, the Netherlands

[2]Lead contact

*Correspondence: p.manganiello@tudelft.nl

https://doi.org/10.1016/j.xcrp.2022.101155

reverse-bias operation, it dissipates large amounts of power, which can lead to formation of hotspots[9] and permanent damage in the PV module. The most common approaches to mitigating these negative effects and improving the shading tolerance of PV modules are adding bypass diodes and connecting strings of solar cells in parallel.[10]

Bypass diodes have been used for decades in the PV industry[11,12] to limit output power loss as well as the power dissipated in reverse-biased solar cells. Most crystalline silicon (c-Si) PV modules in the market include 3 bypass diodes that help to reduce (but not eliminate) the occurrence of hotspots.[13] The shading tolerance of a PV module can be increased by adding more bypass diodes[14] and using bypass elements with low forward voltages.[15] Addition of one bypass diode per cell[16] can virtually reduce the BDV of solar cells to less than 0.5 V.

Parallel interconnections, on the other hand, improve the shading tolerance of PV modules[17] because the voltage of a solar cell varies with the incident irradiance only logarithmically. However, connecting solar cells in parallel can lead to high electrical currents and joule losses at the system level. As a countermeasure, solar cells in PV modules with parallel interconnections are usually cut into smaller pieces to compensate for the total module current.[18,19] The most prominent example of commercial PV modules with parallel interconnections are half-cut solar cell modules.[20–22]

Even though these approaches are effective ways to improve the shading tolerance of PV modules,[23] they also necessitate a more complex manufacturing process. Aiming to simplify module manufacturing and reduce costs, it has been proposed to integrate bypass diodes directly in the structure of the solar cell.[24,25] Although implementation of integrated bypass diodes in front-back contact (FBC) solar cells requires additional fabrication steps and may reduce the active area of the device,[26] developments in interdigitated back contact (IBC) solar cells offer new possibilities.[27] In this case, the junction that naturally forms between the back surface field (BSF) and the emitter on the rear side of an IBC solar cell can allow bypassing the solar cell when it is reverse biased.

Although a few research groups and companies have already manufactured IBC solar cells with BDVs as low as 3 V,[28–31] until now, research on IBC structures has primarily focused on increasing the cell conversion efficiency to maximize the energy yield of PV modules. In this work, we explain that improving the reverse characteristics of IBC solar cells is another promising approach to boosting the performance of PV modules by increasing the shading tolerance and limiting the operating temperature of shaded solar cells. With this aim, we first simulate the breakdown characteristics of realistic IBC solar cells endowed with carrier-selective passivating contacts and presenting contiguous p+ and n+ regions. Then we present annual simulations of PV modules to quantify the effect of the BDV of a solar cell on the annual energy yield and the operating temperature of partially shaded PV modules. Finally, we summarize the results of a four-month-long monitoring campaign through which we compare the energy yield of two PV modules made with solar cells with different breakdown characteristics.

RESULTS AND DISCUSSION

Low-BDV IBC solar cells

Although the fabrication process of IBC solar cells is generally more complex than that of FBC solar cells, IBC devices achieve higher conversion efficiencies by

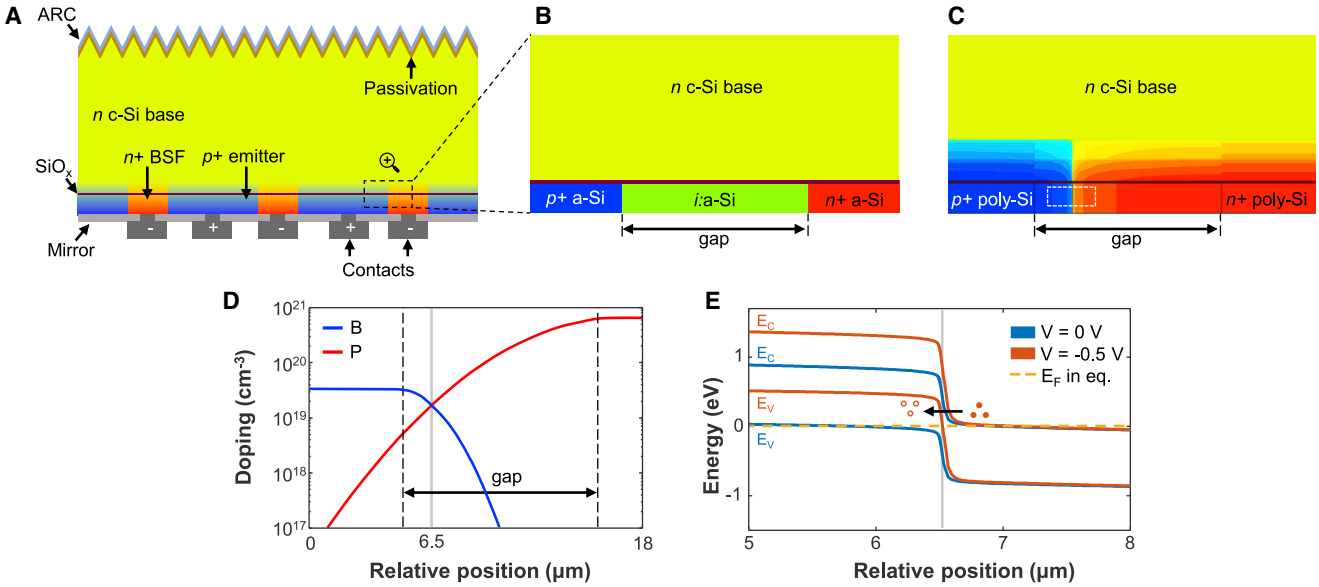

Figure 1. Simulation of IBC solar cells

(A) Analyzed TOPCon IBC solar cell structure.

(B) Close-up view of the region between the back surface field (BSF) and the emitter before crystallization.

(C) Distribution of dopants after crystallization, as simulated in TCAD Sentaurus. The vertical dimension of the figure is stretched to also visualize the penetration of dopant atoms in the c-Si base. The dashed rectangle highlights the portion of the gap investigated in (D) and (E).

(D) Doping profile in the poly-Si region marked with dashed lines in (C). The vertical dashed lines indicate the gap between the p+ and n + fingers before crystallization. The vertical gray solid line indicates the position where the doping profiles meet and polysilicon is compensated.

(E) Band diagrams along the polysilicon region of the IBC cell in the dark under short-circuit and reverse-bias conditions, considering the doping profiles shown in (D). The dashed line represents the Fermi level under short-circuit conditions. In reverse bias, the electrons (filled dots) injected through the negative terminal of the cell recombine through tunneling with holes (empty dots) in the p+ side.

eliminating optical losses caused by the front metallic grid.[32–34] This study focuses on the effects of the BDV on the annual energy yield of PV modules, considering the IBC structure with poly-Si/SiO_x contacts shown in Figure 1A. This is the so-called tunneling oxide passivating contact (TOPCon) technology. Typically, in IBC solar cells based on TOPCon technology,[35,36] the emitter and the BSF regions are physically isolated to prevent shunting because of diffusion of dopant atoms into the c-Si base during the thermal processing steps.[37] However, it has been experimentally demonstrated that it is possible to design highly efficient TOPCon IBC cells with contiguous BSF and emitter regions, where the p+ and n+ fingers are separated by a compensated poly-Si region,[38] forming a p-i-n junction.

Despite diffusion and mixing of dopant atoms during the cell processing steps in the emitter and BSF regions, recombination of charge carriers in the p-i-n junction is strongly limited when the solar cell is forward biased.[39] When the cell is reverse biased, the p-i-n junctions facilitate recombination of the electrons injected at the negative terminal with holes in the emitter. In addition to the avalanche breakdown mechanism, the high doping level in the polysilicon gap region also enables tunneling of carriers at low bias voltages. The influence of this p-i-n junction on the forward and reverse I-V characteristics of a solar cell and the energy yield of PV modules is analyzed in the following sections through detailed simulations.

The BDV of a solar cell is often given as a negative value because the breakdown region of a solar cell is typically represented in the second quadrant of the I-V plane. However, for simplicity, in the following sections we always refer to the magnitude

(absolute value) of the BDV. Consequently, a solar cell with low BDV refers to a device where the voltage drop across the terminals under reverse-bias conditions is as close as possible to 0 V.

BDV simulations

Under low-level injection and forward bias conditions, 1D models can accurately simulate the performance of IBC solar cells.[40] However, for the IBC structure shown in Figure 1A, a 2D model is required to simulate horizontal movement of carriers between the BSF and the emitter.[39] The electrical simulations of solar cells in this work were performed using a 2D finite element model in TCAD Sentaurus, which simultaneously solves the Poisson's equation and the charge carrier transport equations. This model has been validated with respect to homojunction, heterojunction, and TOPCon IBC c-Si solar cells.[41–44]

To obtain cells with different BDVs, simulations were performed, considering different widths for the originally intrinsic gap region between the emitter and the BSF illustrated in Figure 1B. It was considered that, during the thermal processing steps in fabrication of an IBC solar cell, the dopant atoms in the BSF and the emitter diffuse toward the i:poly-Si region and the c-Si base. Although the SiO_x layer hinders diffusion of dopant atoms into the c-Si base, dopant atoms can diffuse in the lateral direction rather easily, as depicted in Figures 1C and 1D. In the simulations, the gap width was varied from 15 μm to 6 μm, maintaining the shape of the doping profiles; i.e., the standard deviation of the Gaussian functions that define the doping concentration was kept constant.

Solar cell simulations were adapted from previous studies of numerical simulation of IBC devices[43] to include transport of carriers between the BSF and the emitter. In particular, the band-to-band tunneling effect in this region has been simulated using self-consistent tunneling models.

As mentioned previously, there are two main transport mechanisms that contribute to the BDV: avalanche and tunneling. Of these two transport mechanisms, tunneling is generally dominant when the BDV is lower than about four times the band gap (approximately 4.5 V in Si).[45] The temperature coefficient of the BDV of all simulated cells presented in this work is positive, which also indicates that band-to-band tunneling dominates over avalanche.[30]

The simulated band diagrams in the dark along the poly-Si region in Figure 1E show that, as the solar cells are driven into the reverse-bias operating region, the tunneling barrier reduces, allowing electrons injected by the external circuit into the n+ region to recombine with holes in the p+ region.

In this work, the width of the gap between the BSF and the emitter was reduced to shorten the tunneling distance and obtain cells with lower BDVs. However, the BDV is controlled by the doping profile in the space domain, which is also determined by cell fabrication steps that define the shape of the doping tails (Figure 1D). Therefore, alternative approaches to fabricate a polysilicon region with similar characteristics as those discussed in this work could also result in cells with low BDVs.

The simulation results of solar cells with different gaps are summarized in Figure 2. Two important trends are identified as the gap between the BSF and the emitter is reduced. A smaller gap implies a shorter tunneling distance in reverse bias, which, in turn, leads to a lower (absolute) BDV, as shown in Figure 2A. At the same time, reducing the (originally)

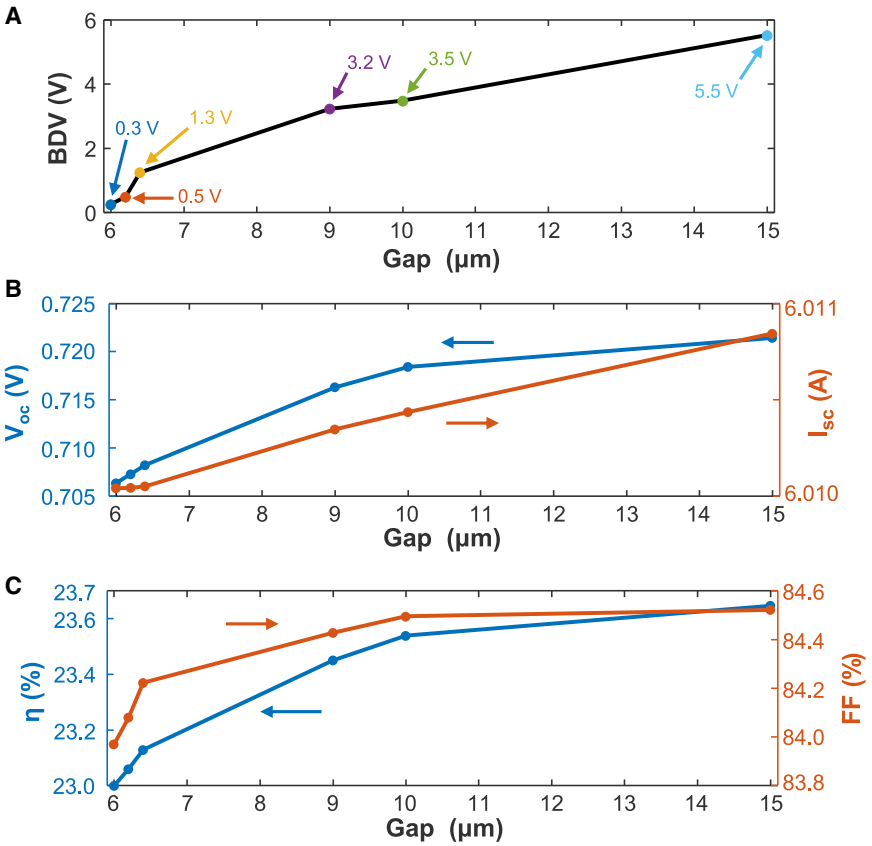

Figure 2. External parameters of the simulated solar cells

(A) BDV of the IBC solar cells in dark at 2 A.

(B) Open-circuit voltage and short-circuit current of IBC cells with different gap widths under STCs.

(C) Efficiency and fill factor of IBC cells with different gap widths under STCs.

i:poly-Si gap results in a higher overlap between heavily doped regions at the bottom of the c-Si base because of vertical diffusion of dopant atoms through the SiO_x layer. This overlap leads to higher recombination and, hence, a reduction in the open-circuit voltage (Figure 2B) and efficiency (Figure 2C) of the solar cell.

It is important to mention that, as the BDV is reduced, the total power dissipated in reverse-bias cells also decreases. The power dissipated in reverse-bias IBC cells can be distributed quite uniformly over its entire area because of the interdigitated structure of the BSF and emitter regions. The combination of these two factors significantly lowers the probability of hotspots (in comparison with FBC solar cells[46]) and allows low-BDV IBC cells to be safely self-bypassed.[47] Unless the number of cells connected in series under the same bypass diode is lower than approximately the cell's BDV divided by the cell's maximum power point voltage, the inclusion of bypass diodes in PV modules with low-BDV solar cells does not provide additional protection against hotspots. Nevertheless, bypass diodes can still help to improve the shading tolerance of the PV module.

Annual energy yield simulations

The trends in efficiency and BDV in Figure 2 have opposing effects on the energy yield of solar modules. Higher efficiencies lead to higher power in forward bias, whereas lower BDVs minimize losses in reverse bias. Each couple efficiency-BDV values

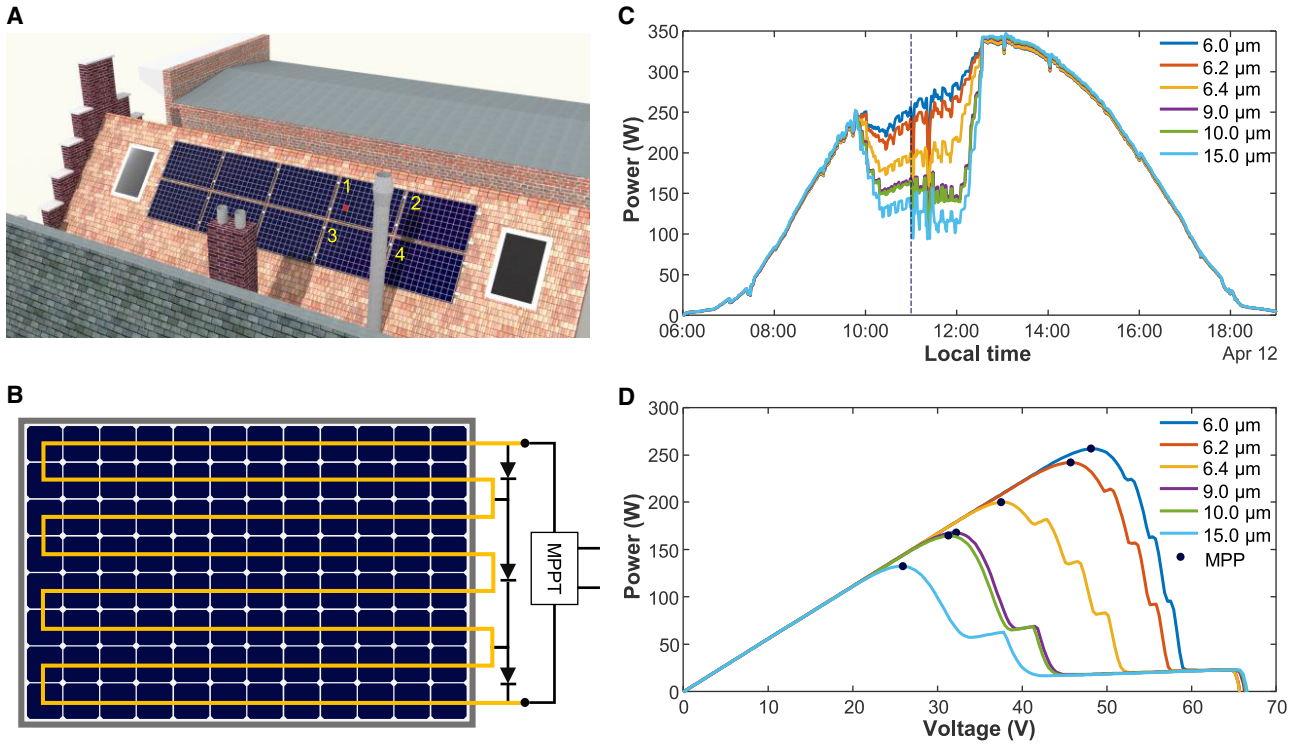

Figure 3. Simulated PV system

(A) CAD model of the simulated PV system on the rooftop of a typical Dutch house.
The rooftop is tilted 50° and facing south. The simulation results correspond to PV module positions 1–4.
(B) Simulated PV module topology. It is assumed that each PV module is connected to a dedicated power converter with maximum power point tracking (MPPT) capability.
(C) Simulated maximum power point time series during a clear-sky day (April 12) for the PV module at rooftop position 1 with cells with different gap widths. The vertical dashed line indicates 11 a.m.
(D) P-V curves of the PV modules with different gap widths at position 1 on April 12 at 11:00 a.m.

corresponds to a certain energy yield that depends on the actual installation and operating conditions. To quantify this, the performance of PV modules under real-world operating conditions has been simulated using a state of the art opto-thermo-electric simulation framework, which enables accurate computation of the temperature and electric power generated (or dissipated) by each solar cell in a PV module.

The performance of PV modules made of solar cells with different gap widths has been simulated considering a PV system on the typical Dutch rooftop, depicted in Figure 3A. The simulation was performed throughout an entire year using 1-min-resolution METEONORM climate data for De Bilt, the Netherlands.[48] The modeling framework deployed here is reported in the supplemental information. Despite the chimneys in front of the PV modules, Table S1 shows that all four modules still receive relatively high levels of irradiation.

The topology of the simulated PV modules, illustrated in Figure 3B, consists of 96 5-in IBC solar cells and 3 Schottky bypass diodes interconnected as in typical commercial PV modules.

The simulated power generated by the PV module in rooftop position 1 during a clear-sky day is presented in Figure 3C. When the module is unshaded, cells with larger gaps deliver slightly more power because of increased cell efficiency.

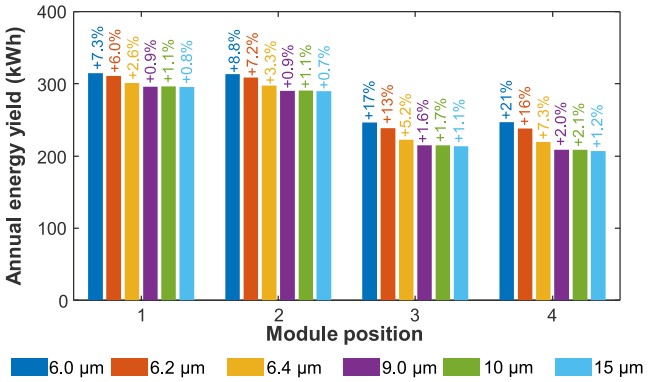

Figure 4. Simulated annual energy yield of PV modules on a typical Dutch rooftop

The percentage above the bars indicates the relative energy yield gain with respect to a PV module made with solar cells that have the same forward characteristics as the cell with a 15-µm gap but with a simulated infinite breakdown, typically more than 10 V or greater than the sum of the open-circuit voltage of the non-shaded cells in the substring.

However, between 10 a.m. and 1 p.m., when the module is partially shaded by one of the chimneys, the advantages of cells with smaller gaps and, thus, low BDVs become clear. The power-voltage (P-V) curves for 11 a.m. in Figure 3D show that cells with smaller gaps achieve higher voltages at the maximum power point under non-uniform illumination but, at the same time, tend to generate multiple local peaks in the P-V curve. Despite the multiple peaks, the results indicate that an MPPT algorithm with 5-min I-V scans would be highly effective at finding the true maximum power point in all simulated cases.

The annual energy yields of the simulated modules are presented in Figure 4. The relative energy yield gain has been calculated, taking as a reference a PV module with solar cells with the same forward characteristics as the cell with a 15-µm gap but an infinite BDV. Because shaded cells with low BDV can be individually bypassed without affecting the power delivered by adjacent unshaded cells, all modules with low-BDV solar cells deliver higher yields than the reference. In most cases, the energy yield loss because of a lower cell efficiency when reducing the gap is overbalanced by energy yield gain because of the reduction in BDV. The energy gain is more noticeable with gaps smaller than 9 µm ($BDV < 3$ V). In particular, the module with cells with a 6-µm gap ($BDV = 0.3$ V) generates over 20% more energy than the reference PV module at rooftop position 4, which is partially shaded about 20% of the time. Although industrial solar cells with $BDV = 2.2$ V have been achieved,[47] the feasibility of manufacturing cost-effective solar cells with BDVs as low as 0.3 V has yet to be demonstrated.

The BDV also influences the thermal performance of reverse-biased solar cells. Figure 5A shows the temperature of the red cell in Figure 3C. Around 11 a.m., when shading occurs, cells with smaller gaps heat up significantly less than cells with larger gaps. One interesting point is that the temperature of the cells with gaps of 6 µm and 6.2 µm drops instead of increasing because the reduction in the absorbed radiation outweighs the power dissipated under reverse bias in the thermal balance. The average and maximum cell temperature during the whole simulated year are presented in Figure 5B. Although the mean annual temperature is approximately constant, it is clear that the maximum cell temperature strongly depends on the reverse breakdown characteristics. These results indicate that solar cells with small gaps can significantly limit the temperature increase because of partial shading, which could

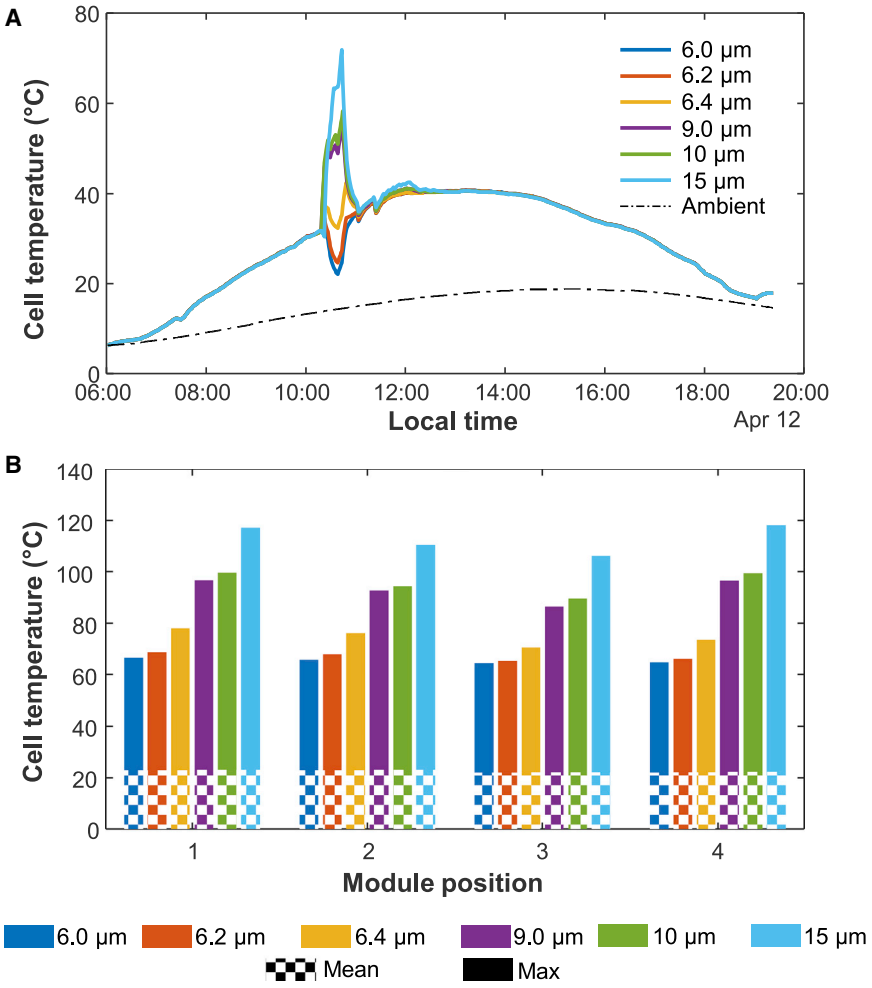

Figure 5. Simulated cell temperature

(A) Temperature profile of the solar cell colored in red in Figure 3A during a clear-sky day.

(B) Mean and maximum temperatures of all cells in the modules during one entire typical meteorological year in the Netherlands.

be beneficial for the PV module's lifetime and reliability and especially relevant to decelerate the degradation of perovskite/silicon tandem PV modules.[49,50]

Figure 4 shows that solar cells with lower efficiency (and lower BDVs) generally imply higher energy yields for PV modules that are mounted on partially shaded rooftops. A different trend is expected for large-scale PV installations because a lower cell efficiency has a much more direct (and negative) effect on energy yield in the absence of shading. However, even in this case, low-BDV solar cells could be preferable because of improved performance under random shading (e.g., because of bird droppings and uneven soiling) and the increased module reliability associated with lower cell temperature peaks.

Experimental validation

Outdoor experiments were performed between May 2021 and August 2021 to validate the simulation framework used in the previous section and measure the effect of BDV on the shading tolerance of PV modules. The two PV modules used during the experiments were laminated in house at the PV module manufacturing unit of Delft

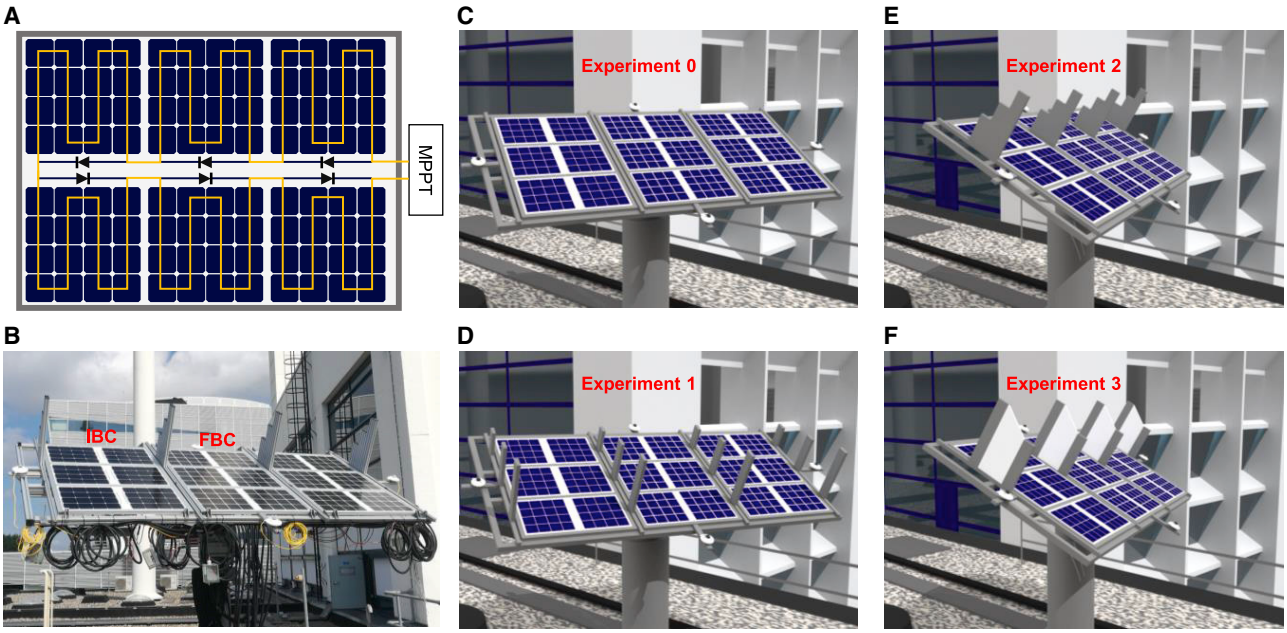

Figure 6. Experimental setup

(A) Layout and electrical interconnection of the manufactured PV modules with 96 solar cells and 6 bypass diodes.

(B) Photograph of the installation with the 2 monitored PV modules.

(C–F) Renderings of the CAD model for each experiment. In all four experiments, the modules were tilted 30°. During experiments 0 and 1, the modules were facing south. During experiments 2 and 3, the modules were facing southeast.

University of Technology and characterized using an A+A+A+ flash solar simulator. Each module consists of 96 solar cells arranged in 6 substrings of 16 series-connected solar cells, where each substring is connected anti-parallel to a Schottky bypass diode, as depicted in Figure 6B. To make a direct comparison between the electrical performance of both PV modules under partial shading, these had to be built with cells of the same size. The first module, referred to as IBC, was built with commercially available 5-in c-Si IBC solar cells with a BDV close to 3 V.[51] The second module, referred to as FBC, was built with 5-in front/back-contacted c-Si Al-BSF solar cells with a BDV larger than 10 V. The external parameters of FBC and IBC cells are listed in Table S2. Even though commercially available FBC solar cells based on passivated emitter and rear contact (PERC) and heterojunction (HJT) technologies can achieve higher efficiencies than Al-BSF, these cells are generally manufactured using 6-in (or larger) wafers and also present BDVs larger than 10 V.[19,52] Taking this into account, it is reasonable to assume that the conclusions from our experiments are also applicable to newer FBC cell technologies.

The two PV modules were installed on a rack at the monitoring station of the Photovoltaic Materials and Devices (PVMD) group in Delft, the Netherlands. The temperature and output power of the PV modules was monitored between May and August 2021 using K-type thermocouples and two LPVO MP1010F-1 maximum power point tracking (MPPT) tracking units,[53] which measured the I-V curves of the PV module every minute and used an MPPT algorithm between I-V sweeps. During this period, the four shading experiments shown in Figures 6C–6F were carried out. In experiment 0, the surroundings of the PV modules were free of obstacles, whereas in experiments 1–3, the PV modules were partially shaded every day by structures attached to the mounting rack.

Along with the measurements, the performance of the PV modules was simulated using the same energy yield framework as in Annual energy yield simulations. Local

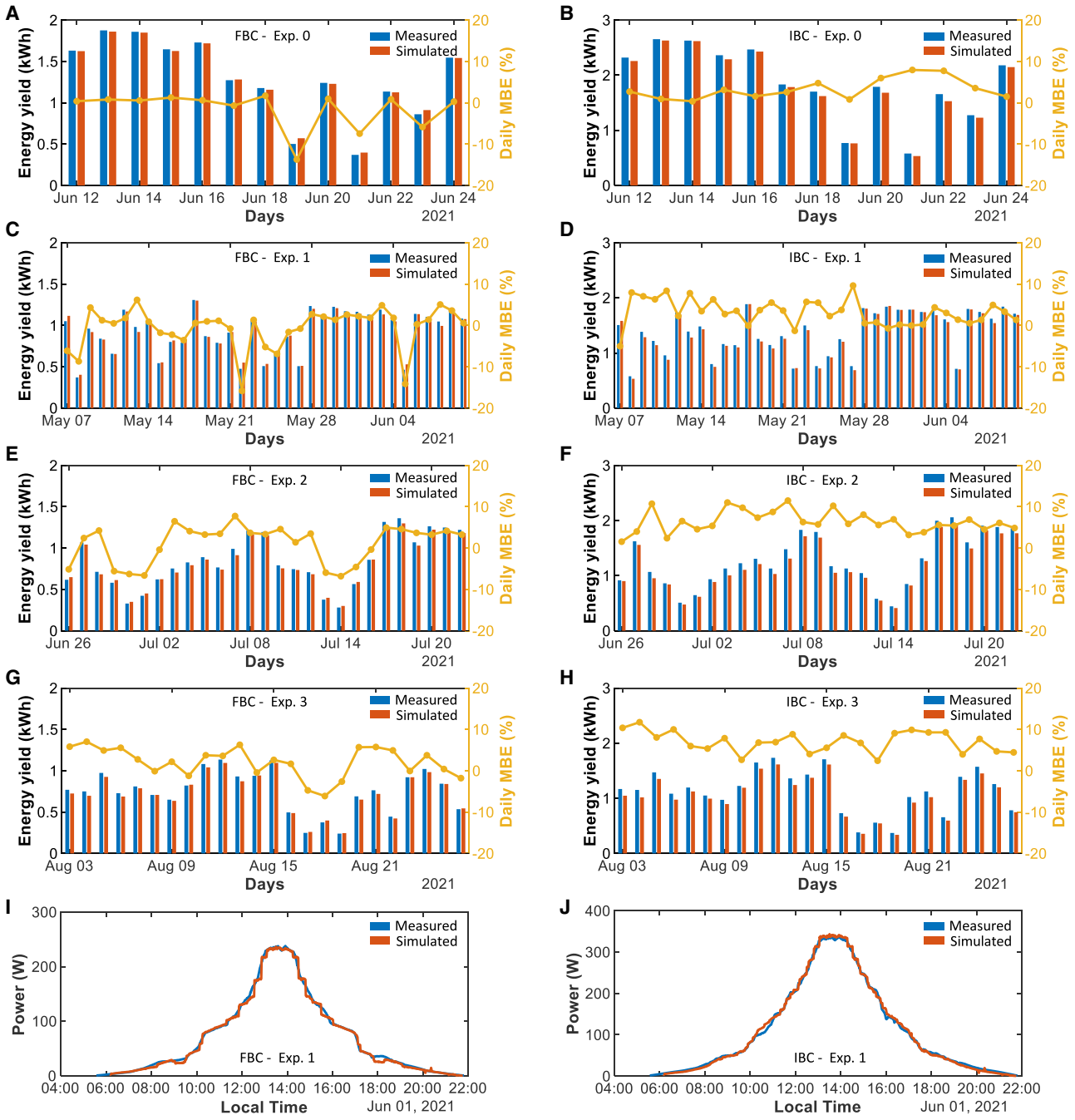

Figure 7. Measured and simulated PV module performance

(A–H) Daily energy yield and mean bias error (MBE) during each of the four shading experiments in Figure 6 for the FBC and the IBC PV modules. (I and J) Maximum power point time series for a clear-sky day during experiment 1 of the FBC and the IBC PV modules.

measurements of the direct normal irradiance (DNI), diffuse horizontal irradiance (DHI), wind speed, and ambient temperature were the only inputs to the numerical simulations. The measured maximum power taken from the measured I-V curves is compared with the simulation results in Figure 7. In general, there is an excellent match between measurements and simulations, and the overall mean bias error (MBE) between the simulated and measured electrical power during the whole

Table 1. Comparison of measured specific yields

	Partially shaded time (%)	FBC yield (Wh/Wp)	IBC yield (Wh/Wp)	Gain (%)
Experiment 0	0	67.0	69.9	4.3
Experiment 1	34	129.7	139.9	7.9
Experiment 2	24	91.0	99.1	9.0
Experiment 3	30	71.8	78.0	8.6

The STC power of the FBC module is 250.6 W, and the STC power of the IBC module is 346.0 W. The gain is calculated by taking the FBC yield as a reference.

experimental campaign was 1.2% and 4.6% for the FBC and the IBC modules, respectively. A detailed comparison of the measured and simulated daily yields is shown in Figures 7A–7H, where the low daily MBE values show the great accuracy of the simulation framework. From the measured and simulated power time series, it can be seen that, during a clear-sky day, the output power profile of the FBC module in Figure 7I is narrower than that of the IBC module in Figure 7J because of the large BDV of the FBC cells and activation of the bypass diodes.

The tested modules differ in BDV and efficiency. Therefore, the energy yield during each experiments was normalized by the power under standard test conditions (STCs) of the corresponding module to quantify the performance improvement because of the BDV. The calculated specific yields are presented in Table 1. During experiment 0, when the modules were unshaded, the specific yield of the IBC module was 4.3% higher than that of the FBC module. This can be explained by considering that (1) the IBC module has a significantly better temperature coefficient than the FBC module; (2) the IBC module operates at slightly lower temperatures because of higher cell efficiency; and (3) the IBC cells have an improved angular response compared with the FBC cells because of improved anti-reflective coating (ARC) and front texturing. During experiments 1–3, when the modules were partially shaded, the relative difference between the specific yield of both modules was, on average, 4.2% higher than in experiment 0. This additional gain in specific yield can be attributed to the improved shading tolerance of the IBC module.

The temperature measurements of shaded solar cells do not show significant differences as in Figure 5A. After a careful analysis, we found that the main reason was failure of the algorithm in the MPPT tracking units to find the true maximum power point when the PV modules were partially shaded. Instead, the modules operated at voltages higher than the maximum power point voltage, and most of the time, the shaded cells were not driven into reverse bias (except during the brief intervals when the I-V curves were traced). This shows that, to benefit from the shading tolerance of PV modules with low BDV and PV modules with many bypass diodes, MPPT algorithms need to be properly engineered to be more effective at finding the global maximum power point.

Finally, after 6 months of continuous operation, the PV modules were measured using an A+A+A+ flash solar simulator and compared with measurements taken prior to the outdoor experiments to verify possible degradation. The measured degradation of the efficiency of the 6 blocks of cells in the IBC module was between 2.0% and 2.5% relative. Although high degradation (up to 10% relative) has been reported in homojunction IBC cells after prolonged operation in strong reverse bias,[54] those testing conditions did not occur during the outdoor experiments presented in this work. Considering that at least two of the blocks of cells in the IBC module in Figure 6 were mostly unshaded, it is likely that different effects (other than operation in reverse bias) also contributed to the degradation of the tested solar cells.[55,56]

The device-level simulation results presented in this article suggest that it is possible to reduce the BDV in TOPCon IBC solar cells by reducing the distance between the emitter and the BSF without creating a shunt. Simulations of partially shaded PV modules indicate that, if the BDV can be reduced to 0.3 V, then the energy yield could be boosted up to 20% for a PV module with 3 bypass diodes that is shaded approximately 20% of the time. We showed that low BDVs allow significant reduction of the temperature increase in reverse-biased solar cells. The simulations results are supported by outdoor experiments showing that, under partial shading conditions, a PV module made with IBC cells with a BDV of 3 V produced an average of 4.2% more energy than a PV module with FBC solar cells with BDVs larger than 10 V and 6 bypass diodes. The findings in this work can be considered additional reasons, beyond high conversion efficiency, to promote market adoption of IBC technology.

EXPERIMENTAL PROCEDURES

Resource availability

Lead contact

Further information and requests for resources and reagents should be directed to and will be fulfilled by the lead contact, Patrizio Manganiello (p.manganiello@tudelft.nl).

Materials availability

This study did not generate new unique materials.

Data and code availability

All data supporting the findings of this study are presented within the article and supplemental information. All other data are available from the lead contact upon reasonable request.

Numerical simulations

Numerical simulations were performed with a state-of-the-art framework developed by the PVMD group. A general flowchart of the simulation framework is presented in Figure S1.

The irradiance incident on the surface of the PV modules was calculated using Radiance,[57] and detailed CAD models of the PV installations. The general approach is described in detail in Calcabrini et al.[58] To improve the accuracy of the results, the spectral distribution of the beam and diffuse and reflected irradiance components were approximated using SBDART[59] for 3 different sky types: clear, partially cloudy, and overcast. To identify the type of sky, the sky classifier presented in Figure S2 was employed.

The absorbed irradiance and generation rate of charge carriers in the solar cell (i.e., the optical generation profiles) were calculated using GenPro4.[60] The effect of temperature on the refractive index of the c-Si bulk was modeled according to Green,[61] and parasitic light absorption in the c-Si base (e.g., because of free carrier absorption) was neglected. The resulting optical generation profiles under different irradiance and temperature conditions were then imported into Technology Computer Aided Design (TCAD) Sentaurus to compute the I-V curve of the solar cell in forward and reverse bias.

In TCAD Sentaurus, the diffusion of dopant atoms in the gap region was modeled with the profile in Figure 1D, which was fitted from measurements on high-efficiency IBC devices.[38]

Table 2. Materials of the laminated PV modules

	FBC	IBC
Front glass	Albarino T 4 mm	Albarino T 4 mm
Front encapsulant	3M EVA9110T	3M EVA9110T
Active layer	Al-BSF mono c-Si 2BB	SunPower Gen III
Rear encapsulant	3M EVA9110T	3M EVA9110T
Backsheet	Icosolar PPF	Icosolar PPF

The I-V curves of the solar cells were simulated under a wide range of temperature and illumination conditions with 5°C and 100 W m^{-2} resolution. Subsequently, the I-V curves calculated with TCAD Sentaurus were interpolated to improve the resolution of the cell's I-V dataset to 1°C and 2 W m^{-2} using cubic Hermite splines.

The I-V curves of the PV module were simulated by adding up the voltage (in series connections) or current (in parallel connections) of the I-V curves of the solar cells simulated with TCAD Sentaurus (or measured, in the case of the experimental setup) and the I-V curves of the bypass diodes. Joule losses in tabbing wires and bus wires were modeled as an increase in the series resistance of the solar cells. Joule losses in wires and connectors were applied to the final PV module I-V curve.

After calculating the I-V curves of the PV modules, the operating point was determined, assuming that each module is connected to a dedicated power converter with an operating voltage range limited to 25–70 V and an MPPT algorithm that performs I-V sweeps every 5 min to find the global maximum in the P-V curve.

The cell temperature was modeled using the 2D thermal model described and validated by Ortiz Lizcano et al.[62] As shown in Figure S1, the thermal model is coupled with the electrical model to account for the electrical power extracted from the solar cells.

Experiments

The PV modules were manufactured using the cells shown in Table S1. The modules were laminated with the recipes shown in Table 2. Prior to the outdoor experiments, the modules were characterized at EternalSun Spire's facilities using an A+A+A+ flash simulator and at the PVMD facilities using a large-area steady-state solar simulator.

During the experiments, I-V curves were measured every minute simultaneously with DNI, DHI, wind speed, and ambient temperature (for the numerical simulations). The PV modules were connected to independent MPPT tracking units (LPVO MP1010F-1) that tracked the maximum power point between I-V sweeps.

Post-experiment degradation measurements were performed at EternalSun Spire's facilities using an A+A+A+ flash simulator calibrated with reference samples that had been measured after lamination and were stored in a dark place (at open circuit) while performing the outdoor experiments.

SUPPLEMENTAL INFORMATION

Supplemental information can be found online at https://doi.org/10.1016/j.xcrp.2022.101155.

ACKNOWLEDGMENTS

This work is supported by the sector plan of the Dutch government in photovoltatronics research. We would like to thank EternalSun Spire (www.eternalsunspire.com), especially Stefan Roest and Elias Garcia Goma (now at www.solarchills.com), for helping us to test the PV modules at EternalSun's facilities.

AUTHOR CONTRIBUTIONS

Conceptualization, A.C. and P.P.M.; methodology, A.C., P.P.M, and P.M.; software, A.C. and P.P.M.; investigation, A.C., P.P.M., B.H., V.K., M.M., and P.M.; resources, A.C., P.P.M., and M.M.; writing – original draft, A.C.; writing – review & editing, P.P.M., B.H., V.K., M.M., P.M., O.I., and M.Z.; supervision, P.M., O.I., and M.Z.

DECLARATION OF INTERESTS

The authors declare no competing interests.

Received: May 3, 2022
Revised: September 7, 2022
Accepted: October 25, 2022
Published: November 22, 2022

REFERENCES

1. Panagiotidou, M., Brito, M.C., Hamza, K., Jasieniak, J.J., and Zhou, J. (2021). Prospects of photovoltaic rooftops, walls and windows at a city to building scale. Sol. Energy *230*, 675–687. https://doi.org/10.1016/j.solener.2021.10.060.

2. Kuhn, T.E., Erban, C., Heinrich, M., Eisenlohr, J., Ensslen, F., and Neuhaus, D.H. (2021). Review of technological design options for building integrated photovoltaics (bipv). Energy Build. *231*, 110381. https://doi.org/10.1016/j.enbuild.2020.110381.

3. Sinapis, K., Rooijakkers, T.T., Pacheco Bubi, R., and van Sark, W.G. (2021). Effects of solar cell group granularity and modern system architectures on partial shading response of crystalline silicon modules and systems. Prog. Photovolt. *29*, 977–989. https://doi.org/10.1002/pip.3420.

4. Centeno Brito, M., Santos, T., Moura, F., Pera, D., and Rocha, J. (2021). Urban solar potential for vehicle integrated photovoltaics. Transport. Res. Transport Environ. *94*, 102810. https://doi.org/10.1016/j.trd.2021.102810.

5. Ziar, H., Manganiello, P., Isabella, O., and Zeman, M. (2021). Photovoltatronics: intelligent pv-based devices for energy and information applications. Energy Environ. Sci. *14*, 106–126. https://doi.org/10.1039/D0EE02491K.

6. Alonso-García, M., and Ruíz, J. (2006). Analysis and modelling the reverse characteristic of photovoltaic cells. Sol. Energy Mater. Sol. Cell. *90*, 1105–1120. https://doi.org/10.1016/j.solmat.2005.06.006.

7. Breitenstein, O., Bauer, J., Bothe, K., Kwapil, W., Lausch, D., Rau, U., Schmidt, J., Schneemann, M., Schubert, M.C., Wagner, J.-M., and Warta, W. (2011). Understanding junction breakdown in multicrystalline solar cells. J. Appl. Phys. *109*, 071101. https://doi.org/10.1063/1.3562200.

8. Clement, C.E., Singh, J.P., Birgersson, E., Wang, Y., and Khoo, Y.S. (2021). Illumination dependence of reverse leakage current in silicon solar cells. IEEE J. Photovolt. *11*, 1285–1290. https://doi.org/10.1109/JPHOTOV.2021.3088005.

9. Simon, M., and Meyer, E.L. (2010). Detection and analysis of hot-spot formation in solar cells. Sol. Energy Mater. Sol. Cell. *94*, 106–113. https://doi.org/10.1016/j.solmat.2009.09.016.

10. Calcabrini, A., Weegink, R., Manganiello, P., Zeman, M., and Isabella, O. (2021). Simulation study of the electrical yield of various pv module topologies in partially shaded urban scenarios. Sol. Energy *225*, 726–733. https://doi.org/10.1016/j.solener.2021.07.061.

11. Swaleh, M., and Green, M. (1982). Effect of shunt resistance and bypass diodes on the shadow tolerance of solar cell modules. Sol. Cell. *5*, 183–198. https://doi.org/10.1016/0379-6787(82)90026-6.

12. Vieira, R., de Araújo, F., Dhimish, M., and Guerra, M. (2020). A comprehensive review on bypass diode application on photovoltaic modules. Energies *13*, 2472. https://doi.org/10.3390/en13102472.

13. Kim, K.A., and Krein, P.T. (2015). Reexamination of photovoltaic hot spotting to show inadequacy of the bypass diode. IEEE J. Photovolt. *5*, 1435–1441. https://doi.org/10.1109/JPHOTOV.2015.2444091.

14. Pannebakker, B.B., de Waal, A.C., and van Sark, W.G. (2017). Photovoltaics in the shade: one bypass diode per solar cell revisited. Prog. Photovolt:. Res. Appl. *25*, 836–849. https://doi.org/10.1002/pip.2898.

15. Bauwens, P., and Doutreloigne, J. (2014). Reducing partial shading power loss with an integrated smart bypass. Sol. Energy *103*, 134–142. https://doi.org/10.1016/j.solener.2014.01.040.

16. Hanifi, H., Pander, M., Jaeckel, B., Schneider, J., Bakhtiari, A., and Maier, W. (2019). A novel electrical approach to protect pv modules under various partial shading situations. Sol. Energy *193*, 814–819. https://doi.org/10.1016/j.solener.2019.10.035.

17. Calcabrini, A., Muttillo, M., Weegink, R., Manganiello, P., Zeman, M., and Isabella, O. (2021). A fully reconfigurable series-parallel photovoltaic module for higher energy yields in urban environments. Renew. Energy *179*, 1–11. https://doi.org/10.1016/j.renene.2021.07.010.

18. Carr, A.J., de Groot, K., Jansen, M.J., Bende, E., van Roosmalen, J., Okel, L., Eerenstein, W., Jonkman, R., van der Sanden, R., Bakker, J., et al. (2015). Tessera: scalable, shade robust module. In IEEE 42nd Photovoltaic Specialist Conference (PVSC) (IEEE), pp. 1–5. 2015. https://doi.org/10.1109/PVSC.2015.7356286.

19. Kunz, O., Evans, R.J., Juhl, M.K., and Trupke, T. (2020). Understanding partial shading effects in shingled pv modules. Sol. Energy *202*, 420–428. https://doi.org/10.1016/j.solener.2020.03.032.

20. Lu, F., Guo, S., Walsh, T.M., and Aberle, A.G. (2013). Improved pv module performance under partial shading conditions. Energy Proc. *33*, 248–255. https://doi.org/10.1016/j.egypro.2013.05.065.

21. Hanifi, H., Schneider, J., and Bagdahn, J. (2015). Reduced shading effect on half-cell modules—measurement and simulation. In 31st European Photovoltaic Solar Energy Conference and Exhibition (EU PVSEC), pp. 2529–2533.

22. Mittag, M., Pfreundt, A., Shahid, J., Wöhrle, N., and Neuhaus, D.H. (2019). Techno-economic analysis of half cell modules: the impact of half cells on module power and costs. In 36th

European Photovoltaic Solar Energy Conference and Exhibition (EU PVSEC), pp. 1032–1039. https://doi.org/10.4229/EUPVSEC20192019-4AV.1.20.

23. Klasen, N., Lux, F., Weber, J., Roessler, T., and Kraft, A. (2022). A comprehensive study of module layouts for silicon solar cells under partial shading. IEEE J. Photovolt. *12*, 546–556. https://doi.org/10.1109/JPHOTOV.2022.3144635.

24. Green, M., Gauja, E., and Withayachamnankul, W. (1981). Silicon solar cells with integral bypass diodes. Sol. Cell. *3*, 233–244. https://doi.org/10.1016/0379-6787(81)90005-3.

25. Suryanto Hasyim, E., Wenham, S., and Green, M. (1986). Shadow tolerance of modules incorporating integral bypass diode solar cells. Sol. Cell. *19*, 109–122. https://doi.org/10.1016/0379-6787(86)90036-0.

26. Chen, K., Chen, D., Zhu, Y., and Shen, H. (2012). Study of crystalline silicon solar cells with integrated bypass diodes. Sci. China Technol. Sci. *55*, 594–599. https://doi.org/10.1007/s11431-011-4712-6.

27. Mulligan, W.P., Rose, D.H., Cudzinovic, M.J., De Ceuster, D.M., McIntosh, K.R., Smith, D.D., et al. (2004). Manufacture of solar cells with 21% efficiency. In 19th European Photovoltaic Solar Energy Conference and Exhibition (EU PVSEC), pp. 387–390.

28. Smith, D.D., Cousins, P.J., Masad, A., Waldhauer, A., Westerberg, S., Johnson, M., Tu, X., Dennis, T., Harley, G., Solomon, G., et al. (2012). Generation iii high efficiency lower cost technology: transition to full scale manufacturing. In 2012 38th IEEE Photovoltaic Specialists Conference (IEEE), pp. 001594–001597. https://doi.org/10.1109/PVSC.2012.6317899.

29. Smith, D.D., Cousins, P.J., Masad, A., Westerberg, S., Defensor, M., Ilaw, R., Dennis, T., Daquin, R., Bergstrom, N., Leygo, A., et al. (2013). Sunpower's maxeon gen iii solar cell: high efficiency and energy yield. In IEEE 39th Photovoltaic Specialists Conference (PVSC) (IEEE), pp. 0908–0913. https://doi.org/10.1109/PVSC.2013.6744291.

30. Chu, H., Koduvelikulathu, L.J., Mihailetchi, V.D., Galbiati, G., Halm, A., and Kopecek, R. (2015). Soft breakdown behavior of interdigitated-back-contact silicon solar cells. Energy Proc. *77*, 29–35. https://doi.org/10.1016/j.egypro.2015.07.006.

31. Müller, R., Reichel, C., Schrof, J., Padilla, M., Selinger, M., Geisemeyer, I., Benick, J., and Hermle, M. (2015). Analysis of n-type ibc solar cells with diffused boron emitter locally blocked by implanted phosphorus. Sol. Energy Mater. Sol. Cell. *142*, 54–59. https://doi.org/10.1016/j.solmat.2015.05.046.

32. Yoshikawa, K., Kawasaki, H., Yoshida, W., Irie, T., Konishi, K., Nakano, K., Uto, T., Adachi, D., Kanematsu, M., Uzu, H., and Yamamoto, K. (2017). Silicon heterojunction solar cell with interdigitated back contacts for a photoconversion efficiency over 26. Nat. Energy *2*, 17032–17038. https://doi.org/10.1038/nenergy.2017.32.

33. Yoshikawa, K., Yoshida, W., Irie, T., Kawasaki, H., Konishi, K., Ishibashi, H., Asatani, T., Adachi, D., Kanematsu, M., Uzu, H., and Yamamoto, K. (2017). Exceeding conversion efficiency of 26% by heterojunction interdigitated back contact solar cell with thin film si technology. Sol. Energy Mater. Sol. Cell. *173*, 37–42. https://doi.org/10.1016/j.solmat.2017.06.024.

34. Hollemann, C., Haase, F., Schäfer, S., Krügener, J., Brendel, R., and Peibst, R. (2019). 26.1%-efficient polo-ibc cells: quantification of electrical and optical loss mechanisms. Prog. Photovolt. Res. Appl. *27*, 950–958. https://doi.org/10.1002/pip.3098.

35. Yang, G., Guo, P., Procel, P., Limodio, G., Weeber, A., Isabella, O., and Zeman, M. (2018). High-efficiency black ibc c-si solar cells with poly-si as carrier-selective passivating contacts. Sol. Energy Mater. Sol. Cell. *186*, 9–13. https://doi.org/10.1016/j.solmat.2018.06.019.

36. Wang, P., Sridharan, R., Ng, X.R., Ho, J.W., and Stangl, R. (2021). Development of topcon tunnel-ibc solar cells with screen-printed fire-through contacts by laser patterning. Sol. Energy Mater. Sol. Cell. *220*, 110834. https://doi.org/10.1016/j.solmat.2020.110834.

37. Reichel, C., Müller, R., Feldmann, F., Richter, A., Hermle, M., and Glunz, S.W. (2017). Influence of the transition region between p-and n-type polycrystalline silicon passivating contacts on the performance of interdigitated back contact silicon solar cells. J. Appl. Phys. *122*, 184502. https://doi.org/10.1063/1.5004331.

38. Hollemann, C., Haase, F., Rienäcker, M., Barnscheidt, V., Krügener, J., Folchert, N., Brendel, R., Richter, S., Großer, S., Sauter, E., et al. (2020). Separating the two polarities of the polo contacts of an 26.1%-efficient ibc solar cell. Sci. Rep. *10*, 658–715. https://doi.org/10.1038/s41598-019-57310-0.

39. Hartenstein, M.B., Stetson, C., Nemeth, W., LaSalvia, V., Harvey, S.P., Theingi, S., Page, M., Jiang, C.-S., Al-Jassim, M.M., Young, D.L., et al. (2021). Trap-assisted dopant compensation prevents shunting in poly-si passivating interdigitated back contact silicon solar cells. ACS Appl. Energy Mater. *4*, 10774–10782. https://doi.org/10.1021/acsaem.1c01775.

40. Verlinden, P.J., Aleman, M., Posthuma, N., Fernandez, J., Pawlak, B., Robbelein, J., Debucquoy, M., Van Wichelen, K., and Poortmans, J. (2012). Simple power-loss analysis method for high-efficiency interdigitated back contact (ibc) silicon solar cells. Sol. Energy Mater. Sol. Cell. *106*, 37–41. https://doi.org/10.1016/j.solmat.2012.06.008.

41. Procel, P., Ingenito, A., De Rose, R., Pierro, S., Crupi, F., Lanuzza, M., Cocorullo, G., Isabella, O., and Zeman, M. (2017). Opto-electrical modelling and optimization study of a novel ibc c-si solar cell. Prog. Photovolt:. Res. Appl. *25*, 452–469. https://doi.org/10.1002/pip.2874.

42. Procel, P., Yang, G., Isabella, O., and Zeman, M. (2018). Theoretical evaluation of contact stack for high efficiency ibc-shj solar cells. Sol. Energy Mater. Sol. Cell. *186*, 66–77. https://doi.org/10.1016/j.solmat.2018.06.021.

43. Procel, P., Yang, G., Isabella, O., and Zeman, M. (2019). Numerical simulations of ibc solar cells based on poly-si carrier-selective passivating contacts. IEEE J. Photovolt. *9*, 374–384. https://doi.org/10.1109/JPHOTOV.2019.2892527.

44. Procel, P., Xu, H., Saez, A., Ruiz-Tobon, C., Mazzarella, L., Zhao, Y., Han, C., Yang, G., Zeman, M., and Isabella, O. (2020). The role of heterointerfaces and subgap energy states on transport mechanisms in silicon heterojunction solar cells. Prog. Photovolt. Res. Appl. *28*, 935–945. https://doi.org/10.1002/pip.3300.

45. Pierret, R.F. (1996). Semiconductor Device Fundamentals (Addison-Wesley Publishing Co.), pp. 264–270. Ch. pn Junction Diode: I-V characteristics.

46. Geisemeyer, I., Fertig, F., Warta, W., Rein, S., and Schubert, M. (2014). Prediction of silicon pv module temperature for hot spots and worst case partial shading situations using spatially resolved lock-in thermography. Sol. Energy Mater. Sol. Cell. *120*, 259–269.

47. Sickmoeller, M. (2020). IBC Technology & Manufacturing (Maxeon Solar Technologies). https://corp.maxeon.com/static-files/c5e8e15e-b191-4bab-96ff-cec504040019.

48. J. Remund, S. Müller, M. Schmutz, D. Barsotti, C. Studer, R. Cattin, Handbook Part I: Software, Meteotest (March 2020).

49. Schwenzer, J.A., Rakocevic, L., Gehlhaar, R., Abzieher, T., Gharibzadeh, S., Moghadamzadeh, S., Quintilla, A., Richards, B.S., Lemmer, U., and Paetzold, U.W. (2018). Temperature variation-induced performance decline of perovskite solar cells. ACS Appl. Mater. Interfaces *10*, 16390–16399. https://doi.org/10.1021/acsami.8b01033.

50. Wolf, E.J., Gould, I.E., Bliss, L.B., Berry, J.J., and McGehee, M.D. (2021). Designing modules to prevent reverse bias degradation in perovskite solar cells when partial shading occurs. Solar RRL *6*, 2100239. https://doi.org/10.1002/solr.202100239.

51. Calcabrini, A., Kambhampati, V., Manganiello, P., Zeman, M., and Isabella, O. (2021). The relevance of the cell's breakdown voltage in the dc yield of partially shaded pv modules. In 2021 IEEE 48th Photovoltaic Specialists Conference (PVSC) (IEEE), pp. 0092–0094. https://doi.org/10.1109/PVSC43889.2021.9518842.

52. Augusto, A., Srinivasa, A., and Bowden, S.G. (2022). Influence of the bulk resistivity on silicon heterojunction solar cells and module reliability. Solar RRL *6*, 2100519. https://doi.org/10.1002/solr.202100519.

53. Jankovec, M., and Topič, M. (2018). LPVO: PV Module Montoring (Meteotest). Accessed 15-Apr-2022. http://lpvo.fe.uni-lj.si/en/services/pv-monitoring/pv-module-monitoring/, online.

54. Chu, H. (2019). Interdigitated Back Contact Silicon Solar Cells: Metallization and Reverse Bias Characteristics, Ph.D. Thesis (International Solar Energy Research Center Konstanz). http://nbn-resolving.de/urn:nbn:de:bsz:352-2-a5lbpuybvl0r5.

55. Müller, R., Reichel, C., Benick, J., and Hermle, M. (2014). Ion implantation for all-alumina ibc solar cells with floating emitter. Energy Proc. *55*, 265–271. https://doi.org/10.1016/j.egypro.2014.08.078.

56. Yamaguchi, S., Van Aken, B.B., Masuda, A., and Ohdaira, K. (2021). Potential-induced degradation in high-efficiency n-type

crystalline-silicon photovoltaic modules: a literature review. Sol. RRL *5*, 2100708. 2100708. https://doi.org/10.1002/solr.202100708.

57. Ward, G.J. (1994). The radiance lighting simulation and rendering system. In Proceedings of the 21st annual conference on Computer graphics and interactive techniques (Siggraph), pp. 459–472.

58. Calcabrini, A., Cardose, R., Gribnau, D., Babal, P., Manganiello, P., Zeman, M., and Isabella, O. (2022). Time-varying, ray tracing irradiance simulation approach for photovoltaic systems in complex scenarios with decoupled geometry, optical properties and illumination conditions. Prog. Photovol. https://doi.org/10.1002/pip.3614.

59. Ricchiazzi, P., Yang, S., Gautier, C., and Sowle, D. (1998). Sbdart: a research and teaching software tool for plane-parallel radiative transfer in the earth's atmosphere. Bull. Am. Meteorol. Soc. *79*, 2101–2114. https://doi.org/10.1175/1520-0477(1998)079%3C2101:SARATS%3E2.0.CO;2.

60. Santbergen, R., Meguro, T., Suezaki, T., Koizumi, G., Yamamoto, K., and Zeman, M. (2017). Genpro4 optical model for solar cell simulation and its application to multijunction solar cells. IEEE J. Photovolt. *7*, 919–926. https://doi.org/10.1109/JPHOTOV.2017.2669640.

61. Green, M.A. (2008). Self-consistent optical parameters of intrinsic silicon at 300 k including temperature coefficients. Sol. Energy Mater. Sol. Cell. *92*, 1305–1310. https://doi.org/10.1016/j.solmat.2008.06.009.

62. Ortiz Lizcano, J.C., Procel, P., Calcabrini, A., Yang, G., Ingenito, A., Santbergen, R., Zeman, M., and Isabella, O. (2021). Colored optic filters on c-si ibc solar cells for building integrated photovoltaic applications. Prog. Photovolt. https://doi.org/10.1002/pip.3504.